Synthesis and Characterization of Double Solid Solution (Zr,Ti) 2 (Al,Sn)C MAX Phase Ceramics

Bensu Tunca, Thomas Lapauw, Rémi Delville, Daniel R. Neuville, Louis Hennet, Dominique Thiaudière, Thierry Ouisse, Joke Hadermann, Jozef Vleugels, Konstantina Lambrinou

Synthesis and characterization of double solid solution $(Zr,Ti)_2(Al,Sn)C$ MAX phase ceramics

Bensu Tunca[a,b,*], *Thomas Lapauw*[b], *Rémi Delville*[a], *Daniel R. Neuville*[c], *Louis Hennet*[d], *Dominique Thiaudière*[e], *Thierry Ouisse*[f], *Joke Hadermann*[g], *Jozef Vleugels*[b] *and Konstantina Lambrinou*[a,h]

[a] SCK•CEN, Boeretang 200, B2400 Mol, Belgium

[b] KU Leuven, Department of Materials Engineering, Kasteelpark Arenberg 44, B-3001 Leuven, Belgium

[c] Géomatériaux, Institut de Physique de Globe de Paris, CNRS-USPC, 75005 Paris, France

[d] CNRS-CEMHTI, Université d'Orléans, 45071 Orléans, France

[e] Synchrotron SOLEIL, L'Orme des Merisiers, Saint-Aubin, 91192 Gif-sur-Yvette, France

[f] Université Grenoble-Alpes, CNRS, Grenoble INP, LMGP, F-38000 Grenoble, France

[g] University of Antwerp, Department of Physics, Electron Microscopy for Materials Research (EMAT), Groenenborgerlaan 171, B-2020 Antwerp, Belgium

[h] Centre for Electron Microscopy and Materials Analysis (EMMA), University of Huddersfield, United Kingdom

Keywords

MAX Phases, Double Solid Solutions, CTE, Lattice Distortions, XRD

Abstract

Quasi phase-pure (>98 wt%) MAX phase solid solution ceramics with the $(Zr,Ti)_2(Al_{0.5},Sn_{0.5})C$ stoichiometry and variable Zr/Ti ratios were synthesized by both reactive hot pressing and pressureless sintering of ZrH_2, TiH_2, Al, Sn, and C powder mixtures. The influence of the different processing parameters, such as applied pressure and sintering atmosphere, on phase purity and microstructure of the produced ceramics was investigated. The addition of Sn to the $(Zr,Ti)_2AlC$ system was the key to achieve phase purity. Its effect on the crystal structure of a 211-type MAX phase was assessed by calculating the distortions of the octahedral M_6C and trigonal M_6A prisms due to steric effects. The M_6A prismatic distortion values were found to be smaller for Sn containing double solid solutions compared to the $(Zr,Ti)_2AlC$ MAX phases. The coefficient of thermal expansion along the <*a*> and <*c*> directions was measured by means of Rietveld refinement of high-temperature synchrotron X-ray diffraction data of $(Zr_{1-x},Ti_x)_2(Al_{0.5},Sn_{0.5})C$ MAX phase solid solutions with x = 0, 0.3, 0.7 and 1. The thermal expansion coefficient data of the $Ti_2(Al_{0.5,}Sn_{0.5})C$ solid solution were compared with those of the Ti_2AlC and Ti_2SnC ternary compounds. The thermal expansion anisotropy increased in the $(Zr,Ti)_2(Al_{0.5},Sn_{0.5})C$ double solid solution MAX phases as compared to the $Zr_2(Al_{0.5},Sn_{0.5})C$ and $Ti_2(Al_{0.5},Sn_{0.5})C$ end-members.

1. Introduction

The MAX phases are an intriguing class of ceramics with metallic-like properties that stem from their nanolaminated crystal structure consisting of M_6X octahedra interleaved with atomic A layers. The MAX phases have the $M_{n+1}AX_n$ general stoichiometry, with n = 1 (211-type), 2 (312-type), or 3 (413-type). The M element corresponds to an early transition metal, A is a group 12-16 element, and X can be either C or N. They are good electrical and thermal conductors, damage tolerant, and machineable like most metals. Some MAX phases are also characterized by an excellent resistance to corrosion, ~~and~~ oxidation and good high-temperature mechanical properties like many ceramics.[1] There are currently around 70

different ternary MAX phases, while the MAX phase family continues to expand steadily either by the discovery of new ternary compounds or the synthesis of higher-order solid solutions.

The synthesis of MAX phase solid solutions allows tailoring of the produced material properties according to the needs of the end application. Substituting M, A and/or X with other elements not only leads to new MAX phases with improved oxidation,[2–6] fracture toughness,[7,8] strength,[4,7] and self-healing properties,[3,9] but also to new ordered structures. Experimental and/or theoretical work on solid solutions revealed the existence of out-of-plane chemically ordered MAX (o-MAX) phases with the $(M_{1/3},M'_{2/3})_3AX_2$ (312) stoichiometry, such as $(Mo_{2/3},Ti_{1/3})_3AlC_2$,[10,11] $(Cr_{2/3},Ti_{1/3})_3AlC_2$,[12–15] $(Ti_{2/3},Zr_{1/3})_3AlC_2$,[16] $(Mo_{2/3}Sc_{1/3})_3AlC_2$,[17] and $(Cr_{1/2},V_{1/2})_3AlC$,[18] as well as $(M_{1/2},M'_{1/2})_4AX_3$ (413) compositions, such as $(Mo_{1/2},Ti_{1/2})_4AlC_3$,[11] $(Cr_{0.5},V_{0.5})_4AlC_3$,[18] and $(Zr_{1/2},Ti_{1/2})_4AlC_3$.[16] In addition to out-of-plane ordering, in-plane-ordered MAX phases (i-MAX) with the $(M_{1/3},M'_{2/3})_2AlC$ stoichiometry were recently discovered, such as $(Cr_{2/3},Sc_{1/3})_2AlC$,[21] $(Cr_{2/3},Y_{1/3})_2AlC$,[19] $(Cr_{2/3},Zr_{1/3})_2AlC$,[20] and $(Mo_{2/3},Sc_{1/3})_2AlC$.[21]

Due to their remarkable properties and versatility ** I don't understand what you want mean by versatility? , the MAX phases are considered for nuclear fuel cladding applications, both for Gen-II/III light water reactors (LWRs) and Gen-IV lead-cooled fast reactors (LFRs). The consideration of the MAX phases for nuclear fuel cladding applications excludes the use of elements with a large neutron cross-section (e.g., Hf, Ta, Mo, Cd, etc.) and focuses on the possible use of elements with small neutron cross-section, such as zirconium (Zr). Moreover, material synthesis should take into account the radiotoxicity of the nuclear waste that must unavoidably be treated/stored at the end of the fuel cycle; therefore, only MAX phase carbides and their solid solutions have so far been considered for fuel cladding applications, as the neutron irradiation of nitrogen (N) generates the long-lived ^{14}C isotope. Another important

consideration with respect to MAX phase synthesis for the nuclear sector is phase purity, so as to mitigate in-service material disintegration due to anisotropic irradiation swelling and/or coefficient of thermal expansion (CTE) mismatch between constituent phases.

High phase purity is also crucial for the determination of the intrinsic properties of the MAX phase ceramics. In earlier work, $(Zr,Ti)_3AlC_2$ and $(Zr,Ti)_2AlC$ solid solution MAX phases were produced with the aim of improving the oxidation resistance of $Zr_{n+1}AlC_n$ MAX phases.[16,22,23] Unfortunately, these solid solution MAX phases had large amounts of secondary phases, similar to the MAX phases produced in the Zr-Al-C system, whereby 67 wt% Zr_2AlC was accompanied by 33 wt% ZrC_x and 61 wt% Zr_3AlC_2 was accompanied by 31 wt% ZrC_x and 8 wt% Al_2Zr.[22,23] Phase-pure Ti-Al-C based MAX phases, on the other hand, have already been reported in literature.[24–26]

Recent work by Lapauw et al. illustrated the improvement of phase purity of Zr_2AlC-based ceramics by partially substituting Zr with Nb and Al with Sn; the produced double 211-type MAX phases solid solutions had the $(Zr_{0.8},Nb_{0.2})_2(Al_{0.5},Sn_{0.5})C$ stoichiometry and contained no rock-salt-like (Nb,Zr)C carbides.[27] These authors associated phase purity with the modification of crystal lattice distortions, due to the creation of solid solutions on both M and A sites in the $M_{n+1}AX_n$ phase compounds. They showed that both Nb and Sn additions decreased the prismatic distortions in the crystal lattice, while the Sn addition increased the octahedral distortion. This steric approach proposed the minimization of the MAX phase lattice distortions by selecting similar-sized M and A atoms, thereby increasing the phase purity of the produced MAX phase ceramics.

The present work investigated the effect of the partial substitution of Al by Sn in the $(Zr,Ti)_2AlC$ MAX phase solid solution. This approach produced quasi phase-pure $(Zr,Ti)_2(Al,Sn)C$ double solid solution MAX phase-based ceramics. The present work also evaluated the effect of the composition and pressureless/pressure-assisted sintering conditions

on phase purity. The resulting microstructure and crystal structure changes of the constituent phases were characterized and their CTEs were measured. The CTE values along <*a*> and <*c*> directions were compared with those of Ti_2AlC[28–30] and Ti_2SnC. Since no CTE*a* and CTE*c* data were available on the Ti_2SnC compound, they were measured on powders from milled Ti_2SnC single crystals.

2. Experimental Section

2.1. Material Synthesis

ZrH_2 (<6 μm, >99% purity, grade G, Chemetall, Germany), TiH_2 (<8 μm, >99% purity, grade V/M, Chemetall, Germany), Al (<5 μm, >99% purity, AEE, United States), Sn (< 5 μm, >99% purity, AEE, United States) and C (<5 μm, >99% purity, Asbury Graphite Mills, United States) powders were used as starting materials for MAX phase synthesis. Specifically, the 211 stoichiometry was targeted in this study, with a (Zr,Ti):(Al,Sn):C starting powder ratio of 2:1.1:0.95. The excess Al was intended to compensate for the partial loss of molten Al during heating (i.e., T_m(Al) ≈ 660°C). The sub-stoichiometric C content was required to compensate for the inward diffusion of C from the graphite die/punch setup during sintering.

The powders were dry mixed in a multidirectional mixer (Turbula type) in polyethylene bottles at 75 rpm for 48 h. Reactive hot pressing (RHP, W100/150-2200-50 LAX, FCT Systeme, Frankenblick, Germany) in vacuum (~10 Pa) was used as reference sintering technology. In addition, four different production routes were studied mainly to investigate their effect on phase purity, crystal structure changes, and lattice distortions. These routes differed in applied pressure (either during cold compaction, CC, or during sintering) and/or the sintering atmosphere, as summarised in **Table 1**. The nomenclature used throughout the text to refer to the different processing routes were: ‘RHP’ for ceramics produced by Reactive

Hot Pressing, RHP, in vacuum, 'Ar' for ceramics pressurelessly sintered in high-temperature furnace (LINN-1800HT, LINN, Eschenfelden, Germany) under flowing argon (Ar, >99.998% purity, ≤ 3 ppm H_2O, ≤ 2 ppm O), and 'CIP' for ceramics Cold Isostatically Pressed (CIP, EPSI, Temse, Belgium).

All sintering routes used a heating rate of 25°C/min, a target temperature of 1450°C and a dwell time of 30 minutes. The dimensions of the ceramics products were: ∅ 30 mm, height ~5 mm for the RHP ceramics, and ∅ 10 mm, height ~5 mm for the CIP ceramics. Since an earlier study[16] revealed relatively large quantities (~60 wt%) of $(Zr,Ti)_2AlC$ phase for a Zr:Ti ratio of 30:70, this Zr:Ti ratio was initially kept constant to assess the influence of the Al:Sn ratio, which varied from 100:0, 90:10, 80:20 to 50:50 for the RHP0 route. An additional set of exploratory samples with a fixed Al:Sn ratio of 90:10 (relatively minor Sn addition) was produced by RHP6/30 with Zr:Ti ratios of 100:0, 80:20, 50:50 and 70:30, and was later used to study the gradual change in lattice distortions as function of the Sn content. Powder batches with a 50:50 Al:Sn ratio, M:A:C ratio of 2:1.1:0.95, and Zr:Ti ratios of 100:0, 70:30, 50:50, 30:70, 0:100 were reactive sintered according to the RHP6/30 and RHP30 routes. Additionally, Zr:Ti ratios of 10:90 and 90:10 were pressurelessly sintered (RHP0, CIP/RHP/0 and CIP/Ar/0), as summarised in **Table 2**.

Table 1. Processing routes used for $(Zr,Ti)_2(Al,Sn)C$ MAX phase synthesis in this work. All ceramics were sintered at 1450°C for 30 min; P = pressure.

	Route	Uniaxial CC (Mpa)	CIP (Mpa)	Sintering Atmosphere	P During Heating (Mpa)	P During Dwell (Mpa)
Pressure-assisted	RHP6/30	30	/	vacuum	6	30
	RHP30	30	/	vacuum	0	30

sintering						
Pressureless sintering	RHP0	30	/	vacuum	0	0
	CIP/RHP/0	/	200	vacuum	0	0
	CIP/Ar/0	/	200	Argon	0	0

Single-phase Ti_2SnC was synthesized as follows: first, single-crystal flakes were grown in a high-temperature solution, whereby Sn and Ti with equal atomic concentrations (Sn:Ti = 1:1) were heated to 1800°C in a closed graphite crucible in an Ar atmosphere. Carbon was provided by high-temperature crucible wall dissolution. After 2 h at 1800°C, the crucible was slowly cooled to 1000°C in 5 days, before stopping the induction heating. Crystals with surface area up to 1 cm^2 were extracted from the solidified flux by etching the latter in highly concentrated HCl. Powder was obtained by ball milling the Ti_2SnC crystals.

2.2. Characterization

Phase identification was performed by X-ray diffraction (XRD) in the 5-75° 2θ range with a step size of 0.02° and a time of 0.2 s per step, using Cu K_α radiation at 30 kV and 10 mA in a Bragg Brentano geometry (X-Ray diffractometer, Bruker D2 Phaser, BRUKER). Measurements were directly performed on the top surface of the ceramic disks, after grinding off the outer carbide layer. The XRD patterns were subjected to Rietveld refinement using the Materials Analysis Using Diffraction (MAUD) software.[31]

Density measurements were done based on the Archimedes principle. Lacquer was used to seal open porosity, thus preventing water penetration into the pores of the produced ceramics. For microstructural characterization, top surfaces of the samples were polished and examined by scanning electron microscopy (SEM, Nova NanoSEM 450, FEI), using backscattered and secondary electron imaging. Electron backscattered diffraction (EBSD) measurements were performed to investigate the effect of applied pressure during sintering on the texture of the

produced ceramics (Nova NanoLab 600 DualBeam, FEI, FIB/SEM equipped with an EBSD detector). The chemical composition of the constituent phases was determined by energy dispersive X-ray spectroscopy (EDS) both in the SEM and the transmission electron microscope (TEM). TEM samples were prepared using a focused ion beam (FIB, Nova NanoLab 600 DualBeam, FEI), using 30 kV Ga ions for milling and 5 kV Ga ions for cleaning. TEM examination was done on a JEOL ARM200F Cs-corrected scanning transmission electron microscope (S/TEM), using selected area diffraction patterns (SAED).

For measuring the CTE of the produced ceramics, high-temperature transmission XRD measurements were done in the DIFFABS beam line at SOLEIL Synchrotron (Paris, France). Measurements on $(Zr_{1-x},Ti_x)_2(Al_{0.5},Sn_{0.5})C$ with x = 0, 0.3, 0.5, 0.7, 1 were done on ceramics that were pressurelessly sintered in vacuum in the hot press (RHP0 in **Table 1**). These sintered MAX phase ceramics were crushed manually in a mortar and loaded into a ∅ 0.5 mm hole pierced in the central flattened section of a ∅ 1 mm PtRh10% heating wire.[32] The confinement of a small powder quantity in such small hole ensures temperature homogeneity. The heating rate was adjusted by manually controlling the current flowing through the Pt wire; the current was calibrated with respect to the corresponding temperature in accordance to a calibration procedure using melting standards. This allowed for measuring in the transmission mode using a focused monochromatic parallel X-ray beam with energy of 17 keV and a wavelength of 0.72932 Å. The diffracted signal was collected with a 2D XPAD detector in the 5-45° 2θ range. A high-purity Ar gas flow prevented excessive oxidation during heating. Measurements were collected from room temperature up to 1500°C in steps of 100°C and at a heating rate of 100°C/min. The powder remained 2 min at each target temperature for data collection. The XRD patterns were subjected to Rietveld refinement using MAUD software.

High-temperature XRD measurements for the determination of the CTE of Ti_2SnC were performed on a Rigaku Smartlab setup equipped with an Anton Paar DHS1100 chamber with a graphite dome. XRD measurements were carried out under nitrogen (N_2) atmosphere in a Bragg-Brentano geometry with a 1D detector with Cu $K\alpha_1$ and Cu $K\alpha_2$ in the 10-150° 2θ range. All XRD patterns were refined using the MAUD software. The refined parameters included the lattice cell parameters *a* and *c*, z_M (i.e., M element z coordinate in the M_2AX unit cell), atomic occupancies for the Zr/Ti and Al/Sn sites, scale parameters and microstrain parameters using the Popa rules[33]. Powder diffraction simulations were done by the POWDERCELL software.[34]

3. Results and Discussion

3.1. Synthesis of $(Zr,Ti)_2(Al_{0.5},Sn_{0.5})C$ MAX Phase Ceramics

The influence of the Sn:Al content on the phase purity of $(Zr,Ti)_2(Al_{1-y},Sn_y)C$ ceramics was initially investigated at a fixed Zr:Ti ratio of 30:70, using the RHP0 processing route. The XRD patterns of the produced $(Zr_{0.3},Ti_{0.7})_2(Al_{1-y},Sn_y)C$ ceramics are presented as a function of the Sn content, y, in **Figure 1a.** Upon increasing the Sn content from y = 0 to 0.5, the content of the competing (Zr,Ti)C carbide and Al-Zr intermetallics, such as Al_2Zr and Al_3Zr, significantly decreased from 39 to 8 wt% for a (Zr,Ti):(Al,Sn):C starting powder stoichiometry of 2:1.2:0.95. Decreasing the content of A elements in the starting powder to 2:1.1:0.95 reduced the fraction of intermetallics below the XRD detection level. Due to the partial substitution of Al by Sn, the characteristic (002) and (004) MAX phase peaks lost most of their intensity, as illustrated by the theoretical powder diffraction simulation of the Zr_2AlC and Zr_2SnC in **Figure 1b**.

With a fixed Sn content (y = 0.5) and overall (Zr,Ti):(Al,Sn):C starting powder stoichiometry of 2:1.1:0.95, 211 MAX phases with various Zr:Ti ratios were successfully synthesized via all

five investigated synthesis routes (**Table 1**). **Figure 1c** and **1d** show representative XRD patterns of $(Zr,Ti)_2(Al_{0.5},Sn_{0.5})C$ ceramics sintered according to route RHP6/30 and RHP0, respectively, as function of the Zr:Ti ratio.

Table 2 summarises the constituent phases of the $(Zr,Ti)_2(Al_{0.5},Sn_{0.5})C$ ceramics, which were determined by XRD Rietveld refinements, as function of composition and synthesis route. For an accurate weight percentage analysis during Rietveld analysis, EDS elemental analysis data from specific phases were used as input for the Zr:Ti and Al:Sn atomic occupancy. The occupancy refinements for the 211 phases hardly deviated from these input values, confirming the overall chemistry of the identified phases. The competing carbide and intermetallic phases showed a limited substitutional solubility for the Zr/Ti and Al/Sn pairs, but the exact compositions of these phases were not studied in detail. However, little or no elemental substitution occurred in the most abundant, competing intermetallic phase Al_2Zr, since its lattice parameters were in agreement with literature data[35] and the EDS elemental maps (**Figure 2**) did not detect significant amounts of Sn and/or Ti. The wt% error in the reported phase assemblies is estimated to be ~1 wt%.

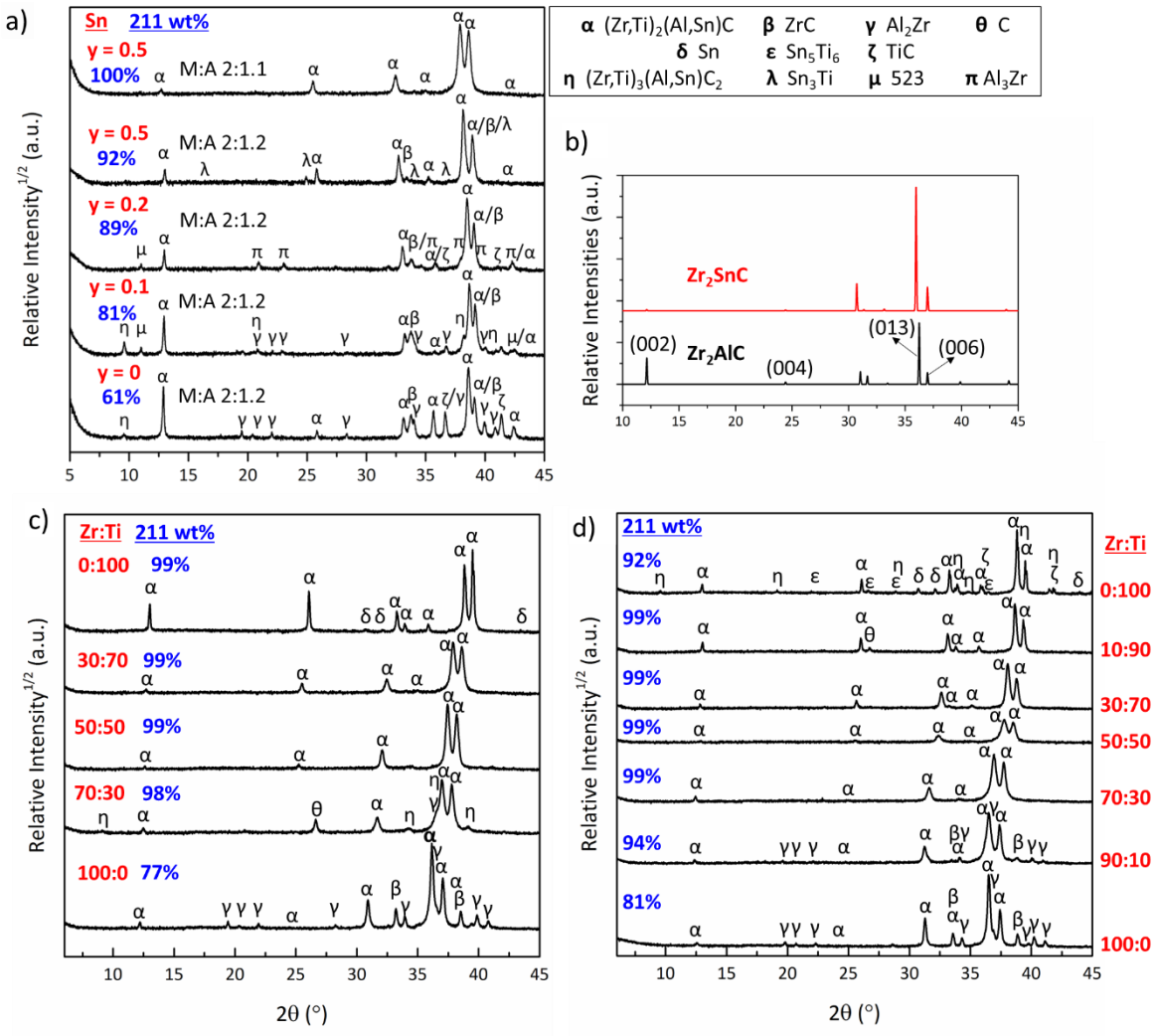

Figure 1. (a) XRD patterns of the $(Zr_{0.3},Ti_{0.7})_2(Al_{1-y},Sn_y)C$ with variable Sn content, y. **(b)** Simulated powder XRD patterns of Zr_2AlC and Zr_2SnC.[22,36] XRD patterns of ceramics with variable Zr:Ti ratio synthesised by the RHP6/30 **(c)** and RHP0 **(d)** processing routes. The 211 MAX phase content, as obtained by Rietveld refinements, is indicated by blue characters.

Note that the detection limit of the XRD technology is around 1-2 wt%. The SEM investigation of produced ceramics indicated as phase-pure by XRD, on the other hand, revealed minor amounts of intermetallics, such as Al_2Zr, as well as Al_2O_3. Image thresholding on greyscale SEM images estimated the content of these minor phases to be 2-3 vol%, and

they were embedded as inclusions in the MAX phase ceramic matrix (see **Figure 2** and **Figure 3**). **Table 2** shows the phase assembly as determined by XRD/Rietveld analysis.

Table 2. Constituent phases of the $(Zr,Ti)_2(Al_{0.5},Sn_{0.5})C$ ceramics as function of composition and synthesis route. Phase assembly determined by XRD Rietveld analysis, where the error in the refined weight percentages is estimated to be ~1 wt%. Ceramics with a proportion of the 211 phase wt% content ≥ 90% are highlighted using bold characters; t.a. = trace amount.

			Phase distribution (wt%)			
Method		**Ti at%**	**211**	**Binary Carbide**	**Intermetallic**	**Others**
RHP6/30	Uniaxial Cold Pressing	0	77	ZrC (8)	Al_2Zr (15)	
		30	**98**		Al_2Zr (t.a.)	312 (2)
	6 MPa during heating	50	**>99**		Al_2Zr (t.a.)	
	30 MPa during dwell	70	**>99**			
	In vacuum	100	**>99**			Sn (t.a.)
RHP30	Uniaxial Cold Pressing	0	66	ZrC (9)		312 (25)
		30	**98**		Al_3Zr_2 (2)	
		50	**>99**		Al_3Zr_2 (t.a.)	
	30 MPa during dwell	70	**>99**			
	In vacuum	100	**>99**			Sn (t.a.)
RHP0	Uniaxial Cold Pressing	0	81	ZrC (7)	Al_2Zr (12)	
		10	**94**	ZrC (2)	Al_2Zr (4)	
		30	**99**		Al_2Zr (t.a.)	
	In vacuum	50	**>99**			
		70	**>99**			
		90	**>99**			
		100	**92**	TiC (4)	Ti_2Sn (t.a.)	312 (2), Sn (2)
CIP/RHP/0	Cold isostatic pressing	0	85	ZrC (10)	Al_2Zr (4), Al_3Zr_2 (t.a.), Sn_3Ti_5 (t.a.)	
		10	**92**	ZrC (8)		
		30	**96**	ZrC (2)	Ti_2Sn (2)	
		50	**98**	ZrC (1), TiC (t.a.)	Ti_2Sn (t.a.)	
	In vacuum	70	**97**	TiC (2)	Ti_2Sn (t.a.)	
		90	**95**	TiC (5)		
		100	68	TiC (10)		312 (22)
CIP/Ar/0	Cold isostatic pressing	0	64	ZrC (9)	Al_2Zr (2), $SnZr_3$ (t.a.)	Al_2O_3 (18), ZrO_2 (7)
		10	84	ZrC (5), TiC (2)	Al_2Zr (7), Ti_2Sn (2)	
		30	**90**	ZrC (3), TiC (t.a.)	Ti_2Sn (t.a.)	312 (2), Sn (5)
		50	84	TiC (3), ZrC (t.a.)	Al_3Zr_2 (2)	Sn (10)
	In Argon	70	86	TiC (3)	Ti_2Sn (t.a.)	312 (t.a.), Sn (8)
		90	89	TiC (3)	Ti_2Sn (t.a.), Sn_3Ti_5 (t.a.)	312 (2), Sn (3)
		100	**98**		Ti_2Sn (t.a.)	312 (t.a.)

All five processing routes allowed synthesizing 211 phase rich ceramics in the Zr-Ti-Al-Sn-C system. $Zr_2(Al_{0.5},Sn_{0.5})C$ proved to be the most challenging phase to produce with high purity,

with a maximum yield of 85 wt% in the CIP/RHP/0 route, with about 10 wt% ZrC, 4 wt% Al_2Zr and trace amounts of other intermetallics. It might be possible to further optimise the phase content by changing the synthesis temperature and dwell time, which were kept constant in this work. With Ti addition up to a Zr:Ti ratio of 50:50, phase purity significantly improved to reach ≥98 wt% for all RHP routes. The occasional intermetallics and Al_2O_3 phases observed by SEM and TEM in the near fully dense ceramics (**Figure 2, Figure 3a** and **3b**) were found to be present at the triple junctions or as thin layers in-between the MAX phase grains.

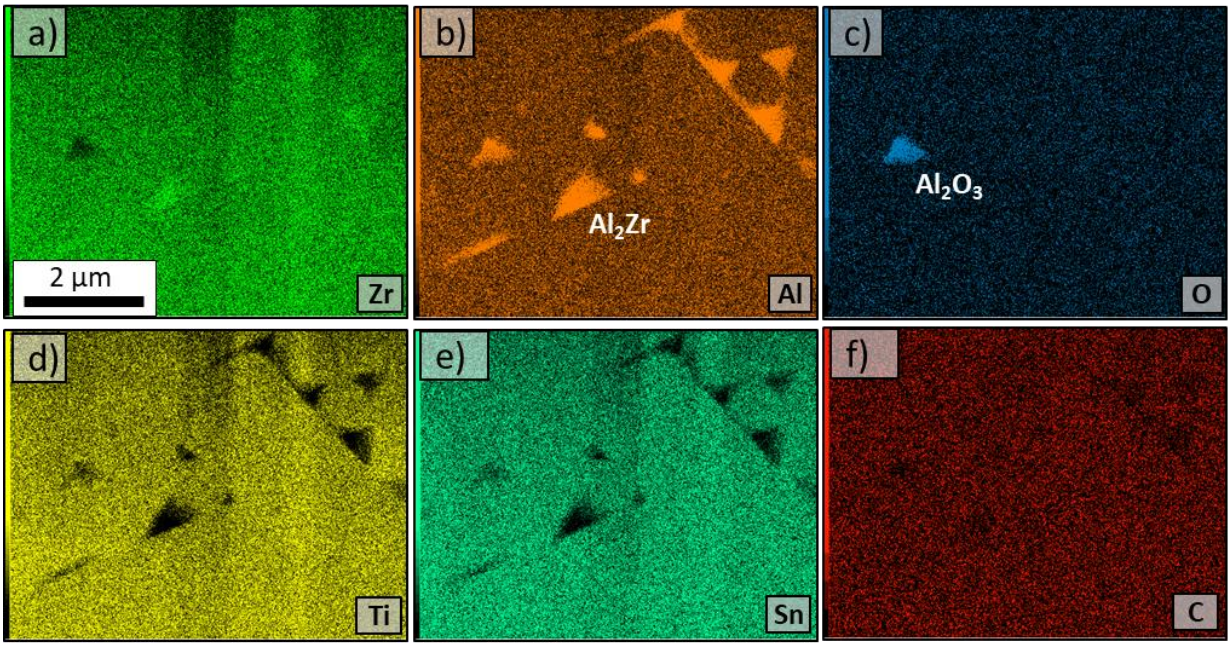

Figure 2. TEM/EDS elemental maps of RHP6/30 $(Zr_{0.5},Ti_{0.5})_2(Al_{0.5},Sn_{0.5})C$ ceramics showing minor inclusions of Al_2Zr and Al_2O_3 phases.

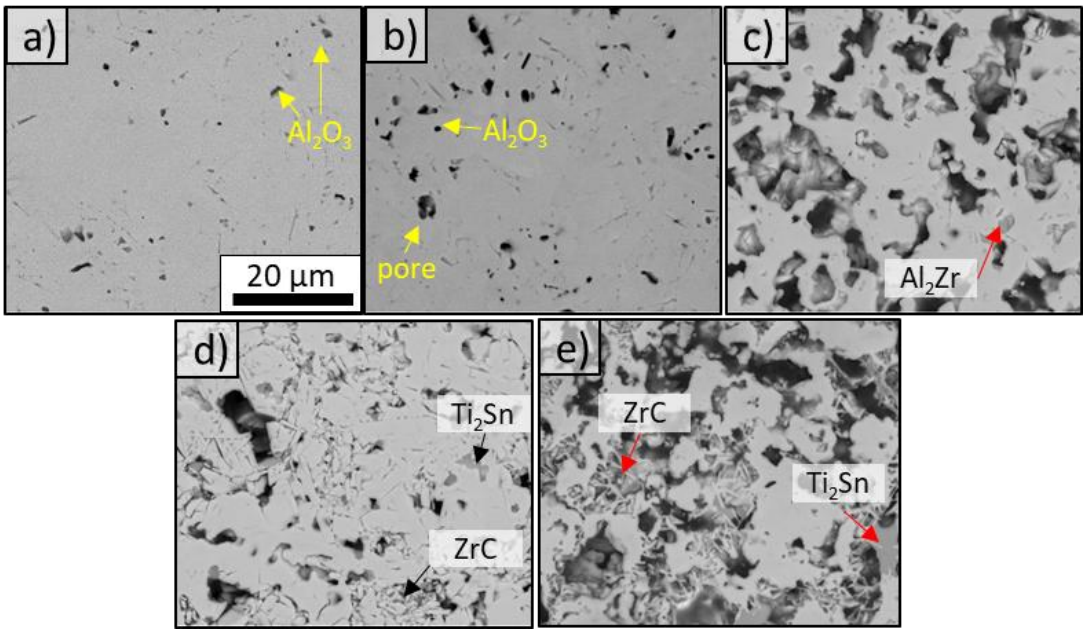

Figure 3. Backscattered SEM images of the porosity in $(Zr_{0.7},Ti_{0.3})_2(Al_{0.5},Sn_{0.5})C$ ceramics as function of the processing route: **(a)** RHP6/30, **(b)** RHP30, **(c)** RHP0, **(d)** CIP/RHP/0 and **(e)** CIP/Ar/0.

The phase purity of the ceramics sintered in vacuum (RHP) was hardly influenced by the selected pressure and loading conditions, indicating that the synthesis of near phase-pure MAX phase ceramics in the $(Zr,Ti)_2(Al,Sn)C$ system is relatively straightforward.

CIPed ceramics always contained up to 10 wt% of binary carbides, the formation of which was not observed in the other processing routes, except for the $Zr_2(Al_{0.5},Sn_{0.5})C$ and $Ti_2(Al_{0.5},Sn_{0.5})C$ end-members This might be due to the higher compaction pressure during CIP that results in a better contact between the carbon and hydrides, limiting the interdiffusivity of molten Al and resulting in more binary carbides. The ceramics sintered in Ar had a substantially lower phase purity than their vacuum-sintered counterparts, except for the $Ti_2(Al_{0.5},Sn_{0.5})C$ composition. This could be attributed to the fact that the Ar trapped in the closed porosity affected the elemental diffusion required for MAX phase formation; this hypothesis is supported by the large isolated bubbles/pores (∅ 40-80 µm) observed in these

ceramics. Moreover, approximately 18 wt% Al_2O_3 and 7 wt% ZrO_2 (monoclinic) were found in the $Zr_2(Al_{0.5},Sn_{0.5})_{1.1}C_{0.95}$ starting powder mixture sintered under Ar flow, indicating that this powder acted as a getter for the oxygen impurities (< 2 ppm) in Ar.

In ceramics containing larger amounts of the Al_2Zr phase, such as the $Zr_2(Al_{0.5},Sn_{0.5})C$ ceramic produced by RHP0, the Al:Sn occupancy in the MAX phase differed from the initial 50:50 ratio resulting in more Sn-rich (Al:Sn ≈ 33:67) 211 phases. In ceramics containing both Zr and Ti, the 211 phases had slightly more Ti than the theoretically targeted value, due to the formation of Al_2Zr or ZrC. In general, increasing the Zr content formed more Al_2Zr, thereby incorporating more Sn in the MAX phase structure. EDS point analyses performed on the produced ceramics showed that the Zr:Ti and Al:Zr ratios in the initial powder mixtures were preserved in the sintered MAX phase ceramics. This is shown in **Table 3** for ceramics synthesised according to the RHP0 processing route.

Table 3. EDS analyses showing the Ti and Sn content in sintered RHP0 $(Zr_{1-x},Ti_x)_2(Al_{1-y},Sn_y)C$ ceramics. The data are tabulated according to the Ti content, x, in the $(Zr_{1-x},Ti_x)_2(Al_{0.5},Sn_{0.5})C$ starting powder mixture. Errors in the refined weight percentages are ~1 wt%.

Initial powder	**Ti (x)**	0	0.1	0.3	0.5	0.7	0.9	1
Sintered 211 MAX Phase	**Ti (x)**	0	0.12(1)	0.32(2)	0.57(4)	0.71(1)	0.92(2)	1
	Sn (y)	0.68(8)	0.63(1)	0.52(5)	0.52(2)	0.57(2)	0.54(2)	0.54(2)
	211 (wt %)	81	94	99	100	100	100	92

Density data of sintered $(Zr_{1-x},Ti_x)_2(Al_{0.5},Sn_{0.5})C$ ceramics as function of composition and processing route are plotted in **Figure 4** along with the theoretical density of the 211 compounds. All RHP6/30 and RHP0/30 grades were nearly fully dense, although limited residual porosity was observed by SEM in some ceramics, such as the one with x_{Ti} = 0.3 produced by RHP30. Ceramics with x_{Ti} = 0.7 grades had, for some unknown reason, a higher porosity. The RHP0, CIP/RHP/0 and CIP/Ar/0 grades had an open porosity of 40-53%, due to the fact that no pressure was applied during sintering. The density of these pressurelessly sintered grades were similar, with RHP0 being slightly higher than the other grades, except for the x_{Ti} = 0 ceramic that contained a considerable amount of the lighter ZrC and Al_2Zr phases. SEM was used to correlate porosity with the processing route study on metallographic cross-sections of $(Zr_{0.7},Ti_{0.3})_2(Al_{0.5},Sn_{0.5})C$ ceramics (**Figure 3**).

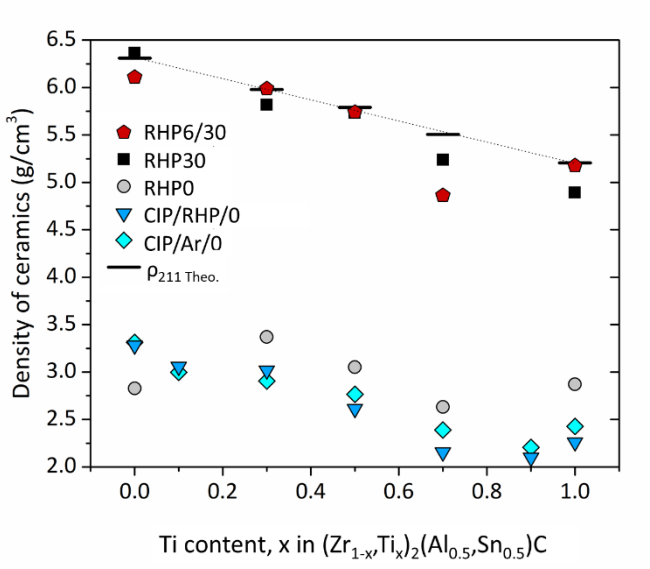

Figure 4. Density of sintered $(Zr_{(1-x)},Ti_x)_2(Al_{0.5},Sn_{0.5})C$ ceramics as function of composition and processing route. The dashed line and horizontal markers represent the theoretical density of the 211 compounds.

The crystal structure of the new MAX phase solid solution was confirmed by TEM on RHP6/30 $(Zr_{0.5},Ti_{0.5})_2(Al_{0.5},Sn_{0.5})C$. The SAED patterns in **Figure 5** show the $[2\bar{1}\bar{1}0]$ and $[1\bar{1}00]$ zone axes of 211 MAX phase grains.

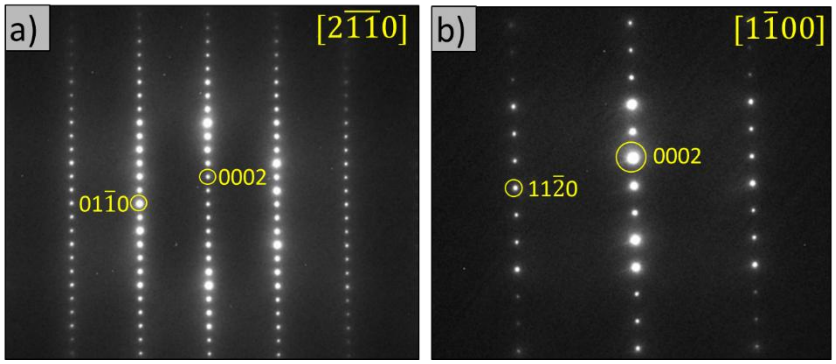

Figure 5. SAED patterns corresponding to the $[2\bar{1}\bar{1}0]$ **(a)** and $[1\bar{1}00]$ **(b)** zone axes of a RHP6/30 $(Zr_{0.5},Ti_{0.5})_2(Al_{0.5},Sn_{0.5})C$ grain.

In terms of microstructure, pressure-assisted sintering resulted in elongated 211 MAX phase lamellae with preferential basal texture. In the pressurelessly sintered ceramics, 211 grains with random orientation were observed, as expected and confirmed by EBSD. The effect of the applied pressure on the texture in the produced ceramics is illustrated in **Figure 6**, which compares the EBSD orientation maps and inverse pole figures of RHP30 and RHP0 $(Zr_{0.7},Ti_{0.3})_2(Al_{0.5},Sn_{0.5})C$ ceramics. EBSD maps were collected from the top surfaces of the ceramic discs; this surfaces were subjected to compressive stresses during processing (i.e., during cold compaction and/or sintering). The dense RHP30 ceramic had a stronger basal texture than the porous RHP0 one, with basal planes aligned parallel to the top disc surface.

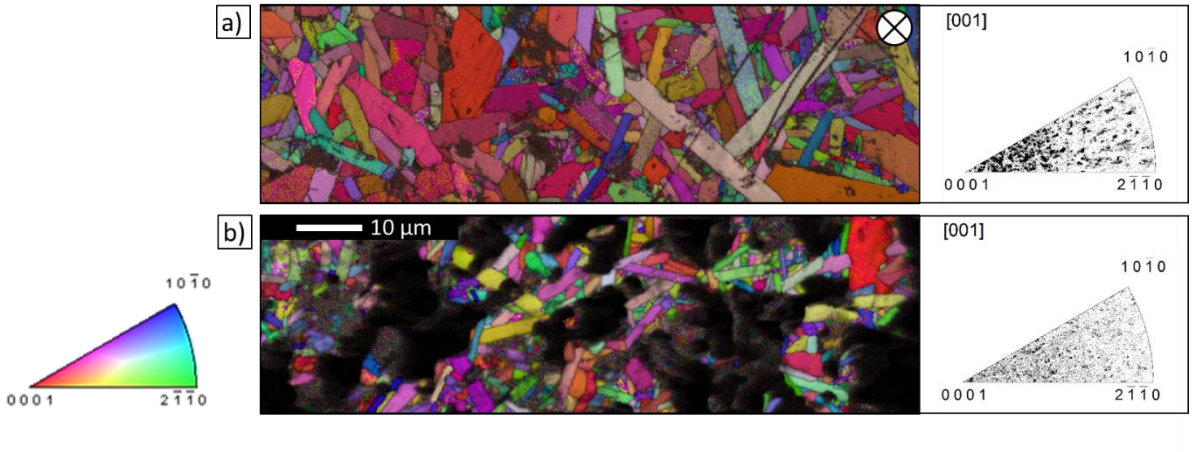

Figure 6. EBSD grain orientation maps and corresponding inverse pole figures of $(Zr_{0.7},Ti_{0.3})_2(Al_{0.5},Sn_{0.5})C$ ceramics produced by **(a)** RHP30 (pressure applied perpendicular to the surface marked by ⊗) and **(b)** RHP0.

3.2. Lattice Parameters and Compliance with Vegard's Law

The lattice parameters *a* and *c* of $(Zr_{1-x},Ti_x)_2(Al_{0.5},Sn_{0.5})C$ ceramics, which were obtained by Rietveld refinement as function of the Ti content, x, are plotted in **Figure 7** (all numerical data are provided in **Table S1** of the supporting information). The uncertainty in lattice parameter determination is estimated to be in the order of 10^{-4} Å. The lattice parameters evolve linearly as function of the Ti content, according to Vegard's law for solid solutions; this holds for all synthesis routes, as shown in **Figure 7a** and **7b**. The relative changes in the lattice parameters, *c/a* ratio, and unit cell volume of ceramics evolve linearly as function of the Ti content, as shown for the $(Zr_{1-x},Ti_x)_2(Al_{0.5},Sn_{0.5})C$ ceramics sintered via RHP6/30 in the **Figure 7d**. The change in average relative z-coordinate of the M-atom in the 211 structure, i.e., the z_M parameter, is shown in **Figure 7c**, also following Vegard's law over the full compositional range, except from a slight deviation at the Ti content of x = 0.3. The lattice parameter evolution of the end-members as function of the Sn:Al ratio is presented in **Figure**

7e. Data for the ternary MAX phases (y = 0 and 1) were taken from literature,[22,28,37,38] whereas the data for the $M_2(Al_{1-y},Sn_y)C$ phases with y = 0.5 were measured experimentally. Although the *a* lattice parameter changes with varying the Al:Sn ratio, the *c* lattice parameter hardly changes.

Overall, the lattice parameters of the double solid solution MAX phases synthesized in this work follow Vegard's law for solid solutions, confirming that Zr and Al can be simultaneously substituted by Ti and Sn. This is no surprise, since $(Zr,Ti)_2AlC$, $Ti_2(Al,Sn)C$ and $Zr_2(Al,Sn)C$ MAX phases have been produced before.[3,16,39] A linear evolution in lattice parameters was observed, irrespective of the processing route (i.e., in both pressureless and pressure-assisted sintering). The lattice parameters, especially the *a* parameter, of the CIP/Ar/0 sintered ceramics produced with a starting powder Ti content of x = 0.3-0.7 appeared to slightly deviate from the other processing routes (see **Figure 7a**), which might be associated to slight variations in the Al:Sn and/or Zr:Ti ratios in these materials.

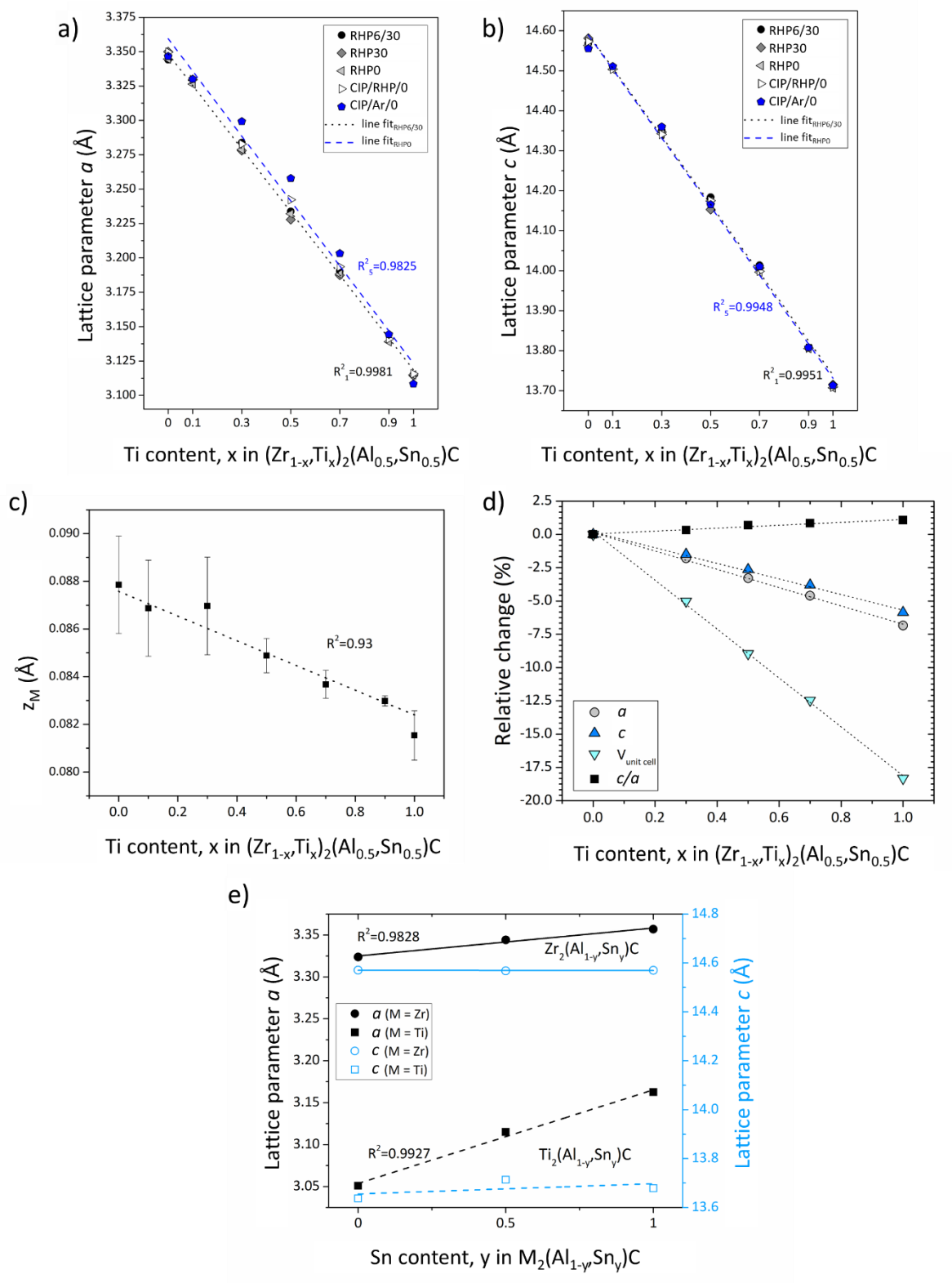

Figure 7. Lattice parameters *a* **(a)** and *c* **(b)** of $(Zr_{1-x},Ti_x)_2(Al_{0.5},Sn_{0.5})C$ as function of the synthesis route. **(c)** Average relative z-coordinate values of the M-atom in the 211 structure, z_M, for all processing routes. **(d)** Relative lattice parameter changes, *c*/*a* ratio, and unit cell

volume for RHP6/30 $(Zr_{1-x},Ti_x)_2(Al_{0.5},Sn_{0.5})C$ as function of the Ti content. **(e)** Lattice parameters *a* and *c* as function of the Sn content, y, in the $M_2(Al_{1-y},Sn_y)C$ ceramics. The values corresponding to ternary MAX phases (y = 0 and 1) were taken from literature.[22,28,37,38,40]

3.3. Lattice Distortions in $(Zr_{1-x},Ti_x)_2(Al_{0.5},Sn_{0.5})C$ MAX Phase Ceramics

The MAX phases are built by alternating M_6X octahedra and M_6A trigonal prisms. Using the refined *a*, *c* and z_M values (with uncertainties of ~10^{-4} Å), the octahedron (O_d)[41] and trigonal prism (P_d)[1,42] distortions of the unit cells can be calculated. The ideal cubic MX octahedron of rock salt structures is distorted in the $M_{n+1}AX_n$ phases; in fact, this octahedral distortion, O_d, can be calculated using the *a*, *c* and z_M for the 211 MAX phase as follows:[41]

$$O_d = \frac{\sqrt{3}}{2\sqrt{4z_M{}^2(\frac{c}{a})^2+\frac{1}{12}}} \qquad (1)$$

Similarly, the distortion of the M_6A trigonal prisms in the 211 structure, P_d, can be calculated from *a*, *c* and z_M as follows:[1,42]

$$P_d = \frac{1}{\sqrt{\frac{1}{3}+(\frac{1}{4}-z_M)^2(\frac{c}{a})^2}} \qquad (2)$$

Ideally, both distortion values are 1 for close-packed spheres in a 211 structure with an ideal *c*/*a* ratio of $2\sqrt{6} \approx 4.89$ and a canonical z_M position of 1⁄12 ≈ 0.0833. When both O_d and P_d values are >1, the *c* axis is under compression. The *a*, *c* and z_M values obtained by Rietveld refinement analysis (see **Figure 7** and **Table S1** in the supporting information) were used to calculate the distortion values. **Figure 8** is a plot of the measured and calculated O_d, P_d values and the O_d/P_d ratio for the RHP6/30 and RHP0 $(Zr_{1-x},Ti_x)_2(Al_{0.5},Sn_{0.5})C$ grades as function of the Ti content, x, along with literature values for the four parent ternary MAX phases (Ti_2AlC, Ti_2SnC, Zr_2AlC and Zr_2SnC), and experimental data on the $(Zr,Ti)_2AlC$[16] and $(Zr,Ti)_2(Al_{0.9},Sn_{0.1})C$ grades. The green shaded areas represent the 211 ceramics with ≥ 90

wt% phase purity (determined by XRD) produced in this study; in fact, these materials are also the only phase-pure ceramics ever produced in the Zr-Ti-Al-Sn-C system. All numerical values and literature data are presented in **Figure S1** of the supporting information.

All calculated O_d and P_d values were >1, indicating compression along the *c* axis. Ti_2SnC had the highest Ti_6C O_d distortion of 1.192, whereas Zr_2AlC[27] had the highest Zr_6Al P_d distortion of 1.101. These values agree with the available literature data.[22,40] The Ti_2SnC distortion values found in literature were not experimentally determined but calculated,[38,40,42] and were added to **Figure 8** along with the values that were experimentally determined in this work. In general, increasing Ti (decreasing Zr) and increasing Sn (decreasing Al) increased O_d. The distortion data of the RHP6/30 and RHP0 $(Zr,Ti)_2(Al_{0.5},Sn_{0.5})C$ grades were comparable. The P_d values evolved in the opposite manner, i.e., decreased with increasing both Ti and Sn, as shown in **Figure 8b**. Substituting Zr by Ti in the $(Zr_{1-x},Ti_x)_2(Al_{1-y},Sn_y)C$ stoichiometry increases O_d and decreases P_d linearly with x. Similarly, substituting Al by Sn up to y = 0.5 increases O_d and decreases P_d at constant x.

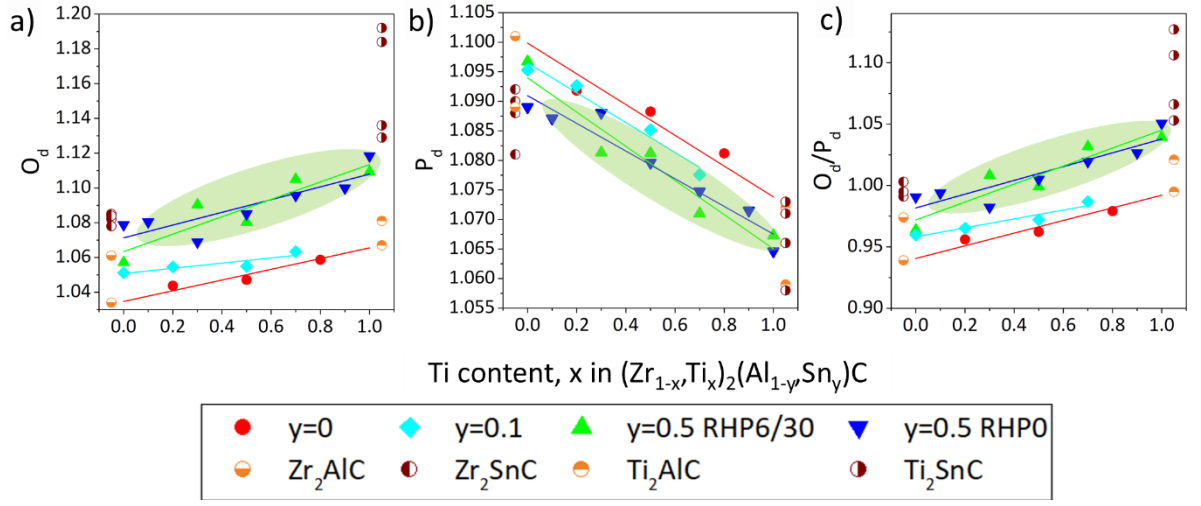

Figure 8. Lattice distortions O_d **(a)**, P_d **(b)** and O_d/P_d ratio **(c)** for the RHP6/30 and RHP0 $(Zr,Ti)_2(Al_{0.5},Sn_{0.5})C$ grades as a function of the Ti content, x, along with literature reference values of the four ternary parent MAX phases[22,27,38,40–43] and experimental data from the

$(Zr,Ti)_2AlC$[16] and $(Zr,Ti)_2(Al_{0.9},Sn_{0.1})C$ grades. The green shaded areas represent the 211 ceramics with ≥ 90 wt% phase purity produced in this study.

The green shaded areas corresponding to phase-pure MAX phases in **Figure 8a** and **8b** are associated with lower P_d and higher O_d values with an O_d/P_d ratio very close to 1.00, as shown in **Figure 8c**. As expected, the solid solution compositions that are located between the end-members have intermediate distortion values. Whereas O_d is smaller in Zr- and Al-rich MAX phases, P_d values are smaller in Ti- and Sn-rich compounds. It is worthwhile noting that the lowest and highest values of the O_d/P_d ratio belong to Zr_2AlC and Ti_2SnC, respectively (**Figure 8c**). While the synthesis of Zr_2AlC produced a ceramic with 33 wt% competing phases (mainly ZrC_x),[22] Ti_2SnC has been synthesized almost phase-pure.[44,45] Ti_2SnC is typically accompanied by Sn minor inclusions that form preferentially at grain boundaries; in this study, Sn was observed at grain boundaries in $Ti_2(Al_{0.5},Sn_{0.5})C$ ceramics sintered at 1450°C. This sintering temperature is high for a Sn-containing MAX phase, considering that the melting point of Sn is very low ($T_m(Sn) \approx 232°C$) and previous studies reported Ti_2SnC decomposition to TiC and Sn at 1250°C.[45] Some applications could benefit from a highly distorted (in O_d) Ti_2SnC with outward diffusing Sn, taking into account that Sn has been reported to have crack self-healing properties in vacuum.[46] Similarly, crack-healing SnO_2 is formed in air when kept at 800°C for 1 h.[47] The green shaded area around $O_d/P_d \approx 1$ in **Figure 8c** ranges from Zr_2SnC to Ti_2AlC. These two ternary MAX phases can be produced phase-pure, as reported in literature,[28,48] while Zr_2AlC with $O_d/P_d \ll 1$ (low O_d and high P_d) suffers from the formation of a competing binary carbide,[22] and Ti_2SnC with $O_d/P_d \gg 1$ (high O_d and low P_d) suffers from outward Sn diffusion and low-temperature degradation.[44,45,49]

Although the data discussed here only represent a small group of the MAX phase family in the Zr-Ti-Al-Sn-C system, it is clear that decreasing the prismatic distortion of the crystal

lattice by substituting Zr by Ti and Al by Sn could be used as a guide for the production of phase-pure 211 MAX phases. The findings of this work support fully the original work of Lapauw et al.,[27] where the aforementioned guidelines were experimentally validated in the Zr-Nb-Al-Sn-C system.

3.4. Thermal Expansion Coefficients (CTEs)

Due to their anisotropic hexagonal crystal structure, the MAX phases are typically characterised by anisotropic thermal expansion, which might trigger microcracking in polycrystalline MAX phase-based ceramics with a non-optimised microstructure. The synthesis of solid solutions could help to tailor the CTE anisotropy of MAX phase-based ceramics, as already reported for $Cr_2(Al_x,Ge_{1-x})C$ ceramics, where an isotropic thermal expansion could be obtained for the $Cr_2(Al_{0.75},Ge_{0.25})C$ stoichiometry.[50] The isotropic CTE of this particular solid solution can be attributed to the fact that the end-members have an opposite thermal expansion behaviour in the *a* and *c* directions, i.e., Cr_2GeC had a larger expansion in the *c* direction, whereas Cr_2AlC had a larger expansion in the *a* direction. Unfortunately, the thermal expansion properties of Zr_2AlC have not yet been reported, whereas to our knowledge only dilatometer-measured CTE data are available for Zr_2SnC and Ti_2SnC.[48] The CTE of Ti_2AlC is well studied and it is higher in the <*c*> direction than in the <*a*> direction, similar to most MAX phases.[28,29]

The experimentally-determined lattice parameter evolution as function of temperature for both $(Zr_{1-x},Ti_x)_2(Al_{0.5},Sn_{0.5})C$ system and Ti_2SnC is given in **Table S2** of the supporting information. The *a* and *c* parameters expanded linearly with temperature, and the CTEs in the <*a*> and <*c*> directions, α_a and α_c, were calculated as follows:

$$\alpha_a = \frac{d(a(T))}{a_0\, dT} \quad \text{and} \quad \alpha_c = \frac{d(c(T))}{c_0\, dT} \qquad (3)$$

whereas the mean CTE[1] was calculated as follows:

$$\alpha_{av} = (2\alpha_a + \alpha_c)/3 \qquad (4)$$

α_a, α_c and α(dilatometer) data existing in literature for Ti_2AlC and Ti_2SnC are plotted in **Figure 9a** together with the respective experimental data obtained for Ti_2SnC and $Ti_2(Al_{0.5},Sn_{0.5})C$ in this work. There is a noticeable discrepancy between the Ti_2AlC CTE values that were reported and those experimentally observed. This could be attributed to the processing route and the phase purity of each material. For example, for one of the data points reported in literature, high-temperature XRD data for the CTE determination was collected from a phase-pure, powder sample.[28] On the other hand, in another study, the sample used was impure, i.e., contained 38±1 wt.% $Ti_5Al_2C_3$ ("523"), 32±1 wt.% Ti_2AlC ("211"), 18±1 wt.% Ti_3AlC_2 ("312"), and 12±1 wt.% $(Ti_{0.5},Al_{0.5})Al$; moreover, this sample was bulk and measured by neutron diffraction.[29] According to **Figure 9a**, Ti_2SnC is almost isotropic with a slightly higher α_a (8.27×10^{-6} K^{-1}) than α_c (8.19×10^{-6} K^{-1}), these values were substantially lower than those determined by dilatometry (10.0×10^{-6} K^{-1}).[48] Although there is some deviation in the available literature data for Ti_2AlC,[28–30] it is safe to claim that the α_c and, by extension, the α_c/α_a ratio of $Ti_2(Al,Sn)C$ decrease with Sn addition.

The α_c/α_a ratio values for the $(Zr_{1-x},Ti_x)_2(Al_{0.5},Sn_{0.5})C$ double solid solutions are plotted in **Figure 9b**, revealing that the thermal expansion anisotropy of the $(Zr_{1-x},Ti_x)_2(Al_{0.5},Sn_{0.5})C$ solid solutions is higher than that of the $Zr_2(Al_{0.5},Sn_{0.5})C$ and $Ti_2(Al_{0.5},Sn_{0.5})C$ end-members.

Both the α_c and the α_a for $(Zr_{1-x},Ti_x)_2(Al_{0.5},Sn_{0.5})C$ are low between x = 0.3 and 0.7 (**Figure 9c**). Due to the failure of the synchrotron measurements on $(Zr_{0.5},Ti_{0.5})_2(Al_{0.5},Sn_{0.5})C$, presumably due to misalignment of the X-ray beam, no CTE data were obtained for this compound. The CTE data plotted as function of composition in **Figure 9b** (numerical data in Table S2 of the supporting information) cannot be fitted with a linear function, as opposed to

what was observed in the $Cr_2(Al_x,Ge_{1-x})C$ system.[50] The linear increase in α_a and α_c in the $Cr_2(Al_x,Ge_{1-x})C$ system with increasing Ge content was accompanied by a linear increase in both O_d and P_d values.

Despite the fact that lattice parameters *c* and *a* decreased linearly and the *c*/*a* ratio increased linearly with increasing Ti content, x, in $(Zr_{1-x},Ti_x)_2(Al_{0.5},Sn_{0.5})C$ (see **Figure 7d**), the CTEs did not evolve linearly as a function of the composition, indicating that they might be affected by the lattice distortions. In fact, it was found that the α_a and α_c values were better fitted with polynomial functions and were accompanied by P_d and O_d with opposite trends as function of the Ti content, x. The CTE minimum in around x = 0.3 might be attributed to the opposite trends in O_d and P_d as a function of x while $O_d/P_d \approx 1$, as shown in **Figure 9c.** Despite the fact that α_c appears rather stable in $(Zr_{1-x},Ti_x)_2(Al_{0.5},Sn_{0.5})C$ compounds with x up to 0.7, the α_a clearly goes through a minimum around x = 0.5 (**Figure 9c**). For all double solid solution MAX phase ceramics, α_c is larger than α_a.

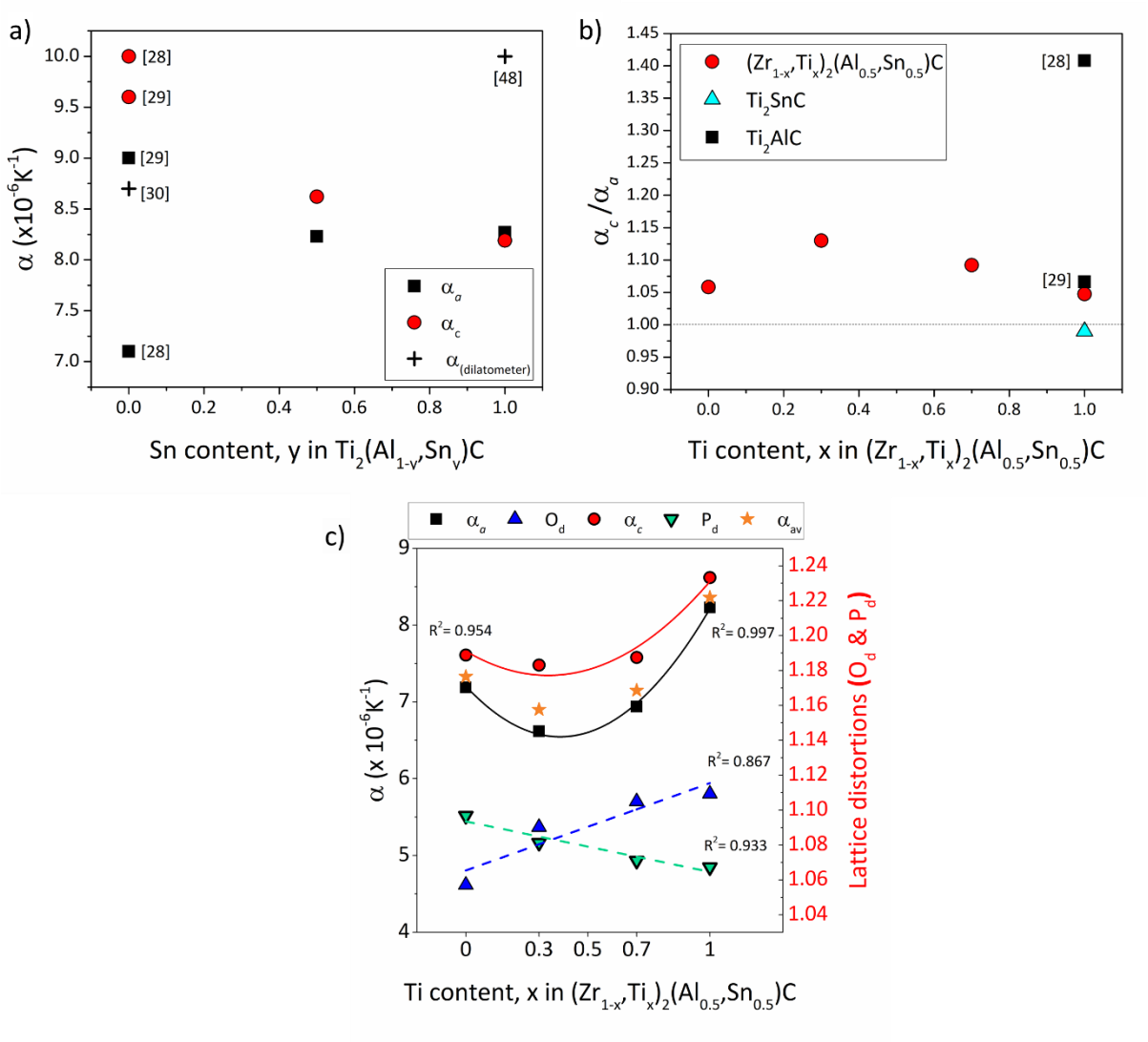

Figure 9. (a) Measured CTE data for $Ti_2(Al_{0.5},Sn_{0.5})C$ and Ti_2SnC, and literature CTE values of the Ti_2AlC and Ti_2SnC end-members[28,29,48,30]). **(b)** α_c/α_a ratios of $(Zr_{1-x},Ti_x)_2(Al_{0.5},Sn_{0.5})C$ solid solutions and $Zr_2(Al_{0.5},Sn_{0.5})C$ and $Ti_2(Al_{0.5},Sn_{0.5})C$ end-members. **(c)** Lattice distortions O_d and P_d for the $(Zr_{1-x},Ti_x)_2(Al_{0.5},Sn_{0.5})C$ solid solutions, as measured by XRD on RHP6/30 ceramics and plotted together with the α_a and α_c values.

4. Conclusions

Near phase-pure (>98 %) $(Zr_{1-x},Ti_x)_2(Al_{0.5},Sn_{0.5})C$ double solid solution MAX phase ceramics with x = 0.1 to 1.0 were synthesized by reactive hot pressing under 30 MPa, as well as by pressureless sintering for 30 min at 1450°C in vacuum. Sintering under vacuum gave better results, irrespective of the applied pressure, as compared to the Ar atmosphere. The hot pressed ceramics were fully densified, whereas the pressurelessly sintered ones had a residual porosity of up to ~50%. XRD phase purity was achieved, while occasional Al_2Zr, Ti_2Sn, Al_3Zr_2 intermetallics, Al_2O_3 and (Zr,Ti)C carbides were identified by SEM as minor phases in the high-purity ceramics.

The *a* and *c* lattice parameters and the relative z-coordinate of the M-atom in the 211 structure, z_M, of the $(Zr_{1-x},Ti_x)_2(Al_{0.5},Sn_{0.5})C$ ceramics decreased linearly with increasing the Ti content, x, following Vegard's law and indicating a complete solid solubility of Zr and Ti at a fixed Al:Sn ratio of 50:50. Similarly, the lattice parameters of $Zr_2(Al_{0.5},Sn_{0.5})C$ and $Ti_2(Al_{0.5},Sn_{0.5})C$ followed Vegard's law with respect to the Zr_2AlC-Zr_2SnC and Ti_2AlC-Ti_2SnC end-members.

The octahedron, O_d, and trigonal prism, P_d, distortions of the lattice in $(Zr_{1-x},Ti_x)_2(Al_{0.5},Sn_{0.5})C$ and $(Zr_{1-x},Ti_x)_2AlC$ solid solutions were calculated from experimental *a*, *c*, and z_M data and were compared with those of ternary end-member data calculated from existing literature data. All 211 solid solution distortions fell within the boundaries of the four Zr_2AlC, Ti_2AlC, Zr_2SnC and Ti_2SnC end-members. The most distorted lattices were found to be Zr_2AlC (highest P_d) and Ti_2SnC (highest O_d). Adding Ti in the $(Zr_{1-x},Ti_x)_2(Al_{1-y},Sn_y)C$ system up to x = 1 increased O_d and decreased P_d, both linearly, whereas adding Sn up to y = 0.5 increased O_d and decreased P_d. Decreasing the trigonal distortion, P_d and approaching to $O_d/P_d \approx 1$, by alloying with both Ti and Sn proved to be key in obtaining phase-pure $(Zr_{1-x},Ti_x)_2(Al_{1-y},Sn_y)C$ MAX phase ceramics.

The α_a and α_c of ternary Ti_2SnC was determined to be 8.27×10^{-6} K^{-1} and 8.19×10^{-6} K^{-1}, respectively, indicating an almost isotropic thermal expansion. The CTE of $(Zr_{1-x},Ti_x)_2(Al_{0.5},Sn_{0.5})C$ with x = 0, 0.3, 0.7, 1 was higher in the *c* direction than in the *a* direction, and evolved through a minimum around x = 0.3, resulting in a concomitant maximum in the α_c/α_a ratio.

In support of the original work of Lapauw et al.,[27] forming double solid solutions improved the phase purity of $(Zr,Ti)_2(Al_{0.5},Sn_{0.5})C$ MAX phase ceramics synthesised via different processing routes (with or without pressure). The synthesis of MAX phase ceramics with high phase purity is an important milestone in assessing the true potential of such innovative materials for nuclear fuel cladding applications by allowing the determination of intrinsic mechanical properties, compatibility with the coolant (corrosion, oxidation) and resistance to irradiation.

ASSOCIATED CONTENT

Supporting Information.

The following files are available free of charge.

Numerical values of CTE, a, z, z_M, O_d, P_d and O_d/P_d of $(Zr_{1-x},Ti_x)_2(Al_{1-y},Sn_y)C$ MAX phases (PDF)

AUTHOR INFORMATION

Corresponding Author

E-mail: btunca@sckcen.be

ORCID

Bensu Tunca 0000-0001-8611-3636

Author Contributions

B.T., main author, conducted most of the experiments. T.L., co-author, assisted in the experimental part. D.R.N., L.H., D.T. and R.D. contributed to the high-temperature synchrotron experiments. T.O. for conduction/supervision of Ti_2SnC single-crystal production and high-temperature XRD measurements. R.D., J.H., J.V. & K.L. for supervision of the scientific work and revision of the manuscript. All authors have approved the final version of the manuscript.

Notes

The authors declare no competing interests.

ACKNOWLEDGEMENTS

H. Roussel and D. Pinek are acknowledged for the Ti_2SnC single-crystal production and high-temperature XRD measurements performed at Grenoble INP-LMGP-CMTC. This research was funded partly by the European Atomic Energy Community's (Euratom) Seventh Framework Programme FP7/2007-2013 under grant agreement No. 604862 (FP7 MatISSE), and partly by the Euratom research and training programme 2014-2018 under grant agreement No. 740415 (H2020 IL TROVATORE). T. Lapauw thanks the Agency for Innovation by Science and Technology (IWT), Flanders, Belgium, for PhD Grant No. 131081. B. Tunca acknowledges the financial support of the SCK•CEN Academy for Nuclear Science and Technology. All authors gratefully acknowledge Synchrotron SOLEIL for the allocated time at the DIFFABS beamline in association with project 20161410 entitled “Investigation of (Zr-Ti)-Al-C MAX phases with in-situ high-temperature XRD”, and the Hercules Foundation for project AKUL/1319 (CombiS(T)EM).

REFERENCES

(1) Barsoum, M. W. MAX Phases Properties of Machinable Ternary Carbides and Nitrides; WILEY-VCH Verlag GmbH & Co. KGaA, **2013**.

(2) Salama, I.; El-Raghy, T.; Barsoum, M. W. Oxidation of Nb_2AlC and $(Ti,Nb)_2AlC$ in Air. J. Electrochem. Soc. **2003**, 150 (3), C152-C158.

(3) Bei, G.; Pedimonte, B.-J.; Fey, T.; Greil, P. Oxidation Behavior of MAX Phase $Ti_2Al_{(1-x)}Sn_xC$ Solid Solution. J. Am. Ceram. Soc. **2013**, 96 (5), 1359–1362.

(4) Gu, J.; Pan, L.; Yang, J.; Yu, L.; Zhang, H.; Zou, W.; Xu, C. Mechanical Properties and Oxidation Behavior of Ti-Doped Nb_4AlC_3. J. Eur. Ceram. Soc. **2016**, 36, 1001–1008.

(5) Zhang, H. B.; Zhou, Y. C.; Bao, Y. W.; Li, M. S. Improving the Oxidation Resistance of Ti_3SiC_2 by Forming a $Ti_3Si_{0.9}Al_{0.1}C_2$ Solid Solution. Acta Mater. **2004**, 52, 3631–3637.

(6) Zhou, Y.; Zhang, H.; Liu, M.; Wang, J.; Bao, Y. Preparation of TiC Free Ti_3SiC_2 with Improved Oxidation Resistance by Substitution Of Si with Al. Mater. Res. Innov. **2004**, 8 (2), 97–102.

(7) Yu, W.; Li, S.; Sloof, W. G. Microstructure and Mechanical Properties of a $Cr_2Al(Si)C$ Solid Solution. Mater. Sci. Eng. A **2010**, 527 (21–22), 5997–6001.

(8) Lapauw, T.; Tytko, D.; Vanmeensel, K.; Huang, S.; Choi, P.-P.; Raabe, D.; Caspi, E. N.; Ozeri, O.; to Baben, M.; Schneider, J. M.; Lambrinou, K.; Vleugels, J. $(Nb_x, Zr_{1-x})_4AlC_3$ MAX Phase Solid Solutions: Processing, Mechanical Properties, and Density Functional Theory Calculations. Inorg. Chem. **2016**, 55 (11), 5445–5452.

(9) Berger, O.; Leyens, C.; Heinze, S.; Baben, M.; Schneider, J. M. Self-Healing of Yttrium-Doped Cr_2AlC MAX Phase Coatings Deposited by HIPIMS. Proc. 4th Int. Conf. Self-healing Mater. (ICSHM 2013) **2013**, 319–323.

(10) Anasori, B.; Halim, J.; Lu, J.; Voigt, C. A.; Hultman, L.; Barsoum, M. W. Mo_2TiAlC_2: A New Ordered Layered Ternary Carbide. Scr. Mater. **2015**, 101, 5–7.

(11) Anasori, B.; Dahlqvist, M.; Halim, J.; Moon, E. J.; Lu, J.; Hosler, B. C.; Caspi, E. N.; May, S. J.; Hultman, L.; Eklund, P.; Rosén, J.; Barsoum, M. W. Experimental and Theoretical Characterization of Ordered MAX Phases Mo_2TiAlC_2 and $Mo_2Ti_2AlC_3$. J. Appl. Phys. **2015**, 118 (9), 094304.

(12) Liu, Z.; Zheng, L.; Sun, L.; Qian, Y.; Wang, J.; Li, M. $(Cr_{2/3}Ti_{1/3})_3AlC_2$ and $(Cr_{5/8}Ti_{3/8})_4AlC_3$: New MAX-Phase Compounds in Ti-Cr-Al-C System. J. Am. Ceram. Soc. **2014**, 97 (1), 67–69.

(13) Liu, Z.; Wu, E.; Wang, J.; Qian, Y.; Xiang, H.; Li, X.; Jin, Q.; Sun, G.; Chen, X.; Wang, J.; Li, M. Crystal Structure and Formation Mechanism of $(Cr_{2/3}Ti_{1/3})_3AlC_2$ MAX Phase. Acta Mater. **2014**, 73, 186–193.

(14) Horlait, D.; Grasso, S.; Al Nasiri, N.; Burr, P. A.; Lee, W. E. Synthesis and Oxidation Testing of MAX Phase Composites in the Cr-Ti-Al-C Quaternary System. J. Am. Ceram. Soc. **2015**, 690 (36501), 682–690.

(15) Burr, P. A.; Horlait, D.; Lee, W. E. Experimental and DFT Investigation of $(Cr,Ti)_3AlC_2$ MAX Phases Stability. Mater Res Lett **2017**, 5 (3), 144-157.

(16) Tunca, B.; Lapauw, T.; Karakulina, O. M.; Batuk, M.; Cabioc'h, T.; Hadermann, J.; Delville, R.; Lambrinou, K.; Vleugels, J. Synthesis of MAX Phases in the Zr-Ti-Al-C System. Inorg. Chem. **2017**, 56 (6), 3489–3498.

(17) Meshkian, R.; Tao, Q.; Dahlqvist, M.; Lu, J.; Hultman, L.; Rosen, J. Theoretical Stability and Materials Synthesis of a Chemically Ordered MAX Phase, Mo_2ScAlC_2, and Its Two-Dimensional Derivate Mo_2ScC_2 MXene. Acta Mater. **2017**, 125, 476–480.

(18) Caspi, E. N.; Chartier, P.; Porcher, F.; Damay, F.; Cabioc, T. Ordering of (Cr,V) Layers in Nanolamellar $(Cr_{0.5}V_{0.5})_{n+1}AlC_n$ Compounds. Mater. Res. Lett. **2015**, 3 (2), 100–106.

(19) Lu, J.; Thore, A.; Meshkian, R.; Tao, Q.; Hultman, L.; Rosen, J. Theoretical and Experimental Exploration of a Novel In-Plane Chemically Ordered $(Cr_{2/3}M_{1/3})_2AlC$ MAX Phase with M = Sc and Y. Cryst. Growth Des. **2017**, 17 (11), 5704–5711.

(20) Chen, L.; Dahlqvist, M.; Lapauw, T.; Tunca, B.; Wang, F.; Lu, J.; Meshkian, R.; Lambrinou, K.; Blanpain, B.; Vleugels, J.; Rosen, J. Theoretical Prediction and Synthesis of $(Cr_{2/3}Zr_{1/3})_2AlC$ i-MAX Phase. Inorg. Chem. **2018**, 57 (11), 6237-6244.

(21) Tao, Q.; Dahlqvist, M.; Lu, J.; Kota, S.; Meshkian, R.; Halim, J.; Palisaitis, J.; Hultman, L.; Barsoum, M. W.; Persson, O. Å.; Rosen, J. Two-Dimensional $Mo_{1.33}C$ MXene with Divacancy Ordering Prepared from Parent 3D Laminate with in-Plane Chemical Ordering. Nat. Publ. Gr. **2017**, 8, 14949.

(22) Lapauw, T.; Lambrinou, K.; Cabioc'h, T.; Halim, J.; Lu, J.; Pesach, A.; Rivin, O.; Ozeri, O.; Caspi, E. N.; Hultman, L.; Eklund, P.; Rosén, J.; Barsoum, M. W.; Vleugels, J. Synthesis of the New MAX Phase Zr_2AlC. J. Eur. Ceram. Soc. **2016**, 36 (8), 1847–1853.

(23) Lapauw, T.; Halim, J.; Lu, J.; Cabioc'h, T.; Hultman, L.; Barsoum, M. W.; Lambrinou, K.; Vleugels, J. Synthesis of the Novel Zr_3AlC_2 MAX Phase. J. Eur. Ceram. Soc. **2016**, 36 (3), 943–947.

(24) Barsoum, M. W.; Brodkin, D.; El-Raghy, T. Layered Machinable Ceramics for High Temperature Applications. **1997**, 36 (5), 53–541.

(25) Peng, C.; Wang, C. A.; Song, Y.; Huang, Y. A Novel Simple Method to Stably Synthesize Ti_3AlC_2 Powder with High Purity. Mater. Sci. Eng. A **2006**, 428 (1–2), 54–58.

(26) Li, L.; Zhou, A.; Xu, L.; Li, Z.; Wang, L. Synthesis of High Pure Ti_3AlC_2 and Ti_2AlC Powders from TiH_2 Powders as Ti Source by Tube Furnace. J. Wuhan Univ. Technol. Mater. Sci. Ed. **2013**, 28 (5), 882–887.

(27) Lapauw, T.; Tunca, B.; Potashnikov, D.; Pesach, A.; Ozeri, O.; Vleugels, J.; Lambrinou, K. The Double Solid Solution $(Zr,Nb)_2(Al,Sn)C$ MAX Phase: A Steric Stability Approach. Sci. Rep. **2018**, 8 (1), 12801.

(28) Barsoum, M. W.; El-Raghy, T.; Ali, M. Processing and Characterization of Ti_2AlC, Ti_2AlN, and $Ti_2AlC_{0.5}N_{0.5}$. Metall. Mater. Trans. A **2000**, 31 (7), 1857–1865.

(29) Lane, N. J.; Vogel, S. C.; Caspi, ad N.; Barsoum, M. W. High-Temperature Neutron Diffraction and First-Principles Study of Temperature-Dependent Crystal Structures and Atomic Vibrations in Ti_3AlC_2, Ti_2AlC, and $Ti_5Al_2C_3$. J. Appl. Phys. **2013**, 113, 183519.

(30) Barsoum, M. W.; Salama, I.; El-Raghy, T.; Golczewski, J.; Seifert, H. J.; Aldinger, F.; Porter, W. D.; Wang, H. Thermal and Electrical Properties of Nb_2AlC, $(Ti,Nb)_2AlC$ and Ti_2AlC. Metall. Mater. Trans. A **2002**, 33 (9), 2775–2779.

(31) Lutterotti, L., Matthies, S., & Wenk, H. MAUD: A Friendly Java Program for Material Analysis Using Diffraction. CPD Newsl. **1999**, 21, 14–15.

(32) Neuville, D. R.; Hennet, L.; Florian, P.; de Ligny, D. In Situ High-Temperature Experiments. Rev. Mineral. Geochemistry **2014**, 78 (1), 779–800.

(33) Popa, N. C.; IUCr. The (Hkl) Dependence of Diffraction-Line Broadening Caused by Strain and Size for all Laue Groups in Rietveld Refinement. J. Appl. Crystallogr. **1998**, 31 (2), 176–180.

(34) Kraus, W.; Nolzeb, G.; IUCr. POWDER CELL – a Program for the Representation and Manipulation of Crystal Structures and Calculation of the Resulting X-Ray Powder Patterns. J. Appl. Crystallogr. **1996**, 29 (3), 301–303.

(35) Kematick, R. J.; Franzen, H. F. Thermodynamic Study of the Zirconium-Aluminum System. J. Solid State Chem. **1984**, 54 (2), 226–234.

(36) Kanoun, M. B.; Goumri-Said, S.; Reshak, A. H. Theoretical Study of Mechanical, Electronic, Chemical Bonding and Optical Properties of Ti_2SnC, Zr_2SnC, Hf_2SnC and Nb_2SnC. Comput. Mater. Sci. **2009**, 47 (2), 491–500.

(37) Vincent, H.; Vincent, C.; Mentzen, B. F.; Pastor, S.; Bouix, J. Chemical Interaction between Carbon and Titanium Dissolved in Liquid Tin: Crystal Structure and Reactivity of Ti_2SnC with Al. Mater. Sci. Eng. A256 **1998**, 83–91.

(38) Zhou, Y. C.; Dong, H. Y.; Wang, X. H.; Chen, S. Q. Electronic Structure of the Layered Ternary Carbides Ti_2SnC and Ti_2GeC. J. Phys. Condens. Matter **2000**, 12 (46), 9617–9627.

(39) Ali, M. A.; Hossain, M. M.; Jahan, N.; Islam, A. K. M. A.; Naqib, S. H. Newly Synthesized Zr_2AlC, $Zr_2(Al_{0.58}Bi_{0.42})C$, $Zr_2(Al_{0.2}Sn_{0.8})C$, and $Zr_2(Al_{0.3}Sb_{0.7})C$ MAX Phases: A DFT Based First-Principles Study. Comput. Mater. Sci. **2017**, 131, 139–145.

(40) Kanoun, M. B.; Goumri-Said, S.; Jaouen, M. Steric Effect on the M Site of Nanolaminate Compounds M_2SnC (M = Ti, Zr, Hf and Nb). J. Phys. Condens. Matter **2009**, 21 (4), 045404.

(41) Hug, G.; Jaouen, M.; Barsoum, M. W. X-Ray Absorption Spectroscopy, EELS, and Full-Potential Augmented Plane Wave Study of the Electronic Structure of Ti_2AlC, Ti_2AlN, Nb_2AlC and $(Ti_{0.5}Nb_{0.5})_2AlC$. Phys. Rev. B **2005**, 71 (2), 024105.

(42) Hug, G. Electronic Structures of and Composition Gaps among the Ternary Carbides Ti_2MC. Phys. Rev. B - Condens. Matter Mater. Phys. **2006**, 74 (18), 1–7.

(43) Jeitschko, W.; Nowotny, H.; Benesovsky, F. Kohlenstoffhaltige Ternaire Verbindungen (H-Phase). Monatshefte für Chemie **1963**, 332, 2–6.

(44) Barsoum, M. W.; Yaroschuk, G.; Tyagi, S. Fabrication and Characterization of M_2SnC (M = Ti, Zr, Hf and Nb). Scr. Mater. **1997**, 37 (10), 1583–1591.

(45) Li, S. B.; Bei, G. P.; Zhai, H. X.; Zhou, Y. Bimodal Microstructure and Reaction Mechanism of Ti_2SnC Synthesized by a High-Temperature Reaction Using Ti/Sn/C and Ti/Sn/TiC Powder Compacts. J. Am. Ceram. Soc. **2006**, 89 (12), 3617–3623.

(46) Li, S.; Zhang, L.; Yu, W.; Zhou, Y. Precipitation Induced Crack Healing in a Ti_2SnC Ceramic in Vacuum. Ceram. Int. **2017**, 43 (9), 6963–6966.

(47) Li, S.; Bei, G.; Chen, X.; Zhang, L.; Zhou, Y.; Mačkoví, M.; Spiecker, E.; Greil, P. Crack Healing Induced Electrical and Mechanical Properties Recovery in a Ti_2SnC Ceramic. J. Eur. Ceram. Soc. **2016**, 36, 25–32.

(48) El-Raghy, T.; Chakraborty, S.; Barsoum, M. W. Synthesis and Characterization of Hf_2PbC, Zr_2PbC and M_2SnC (M = Ti, Hf, Nb or Zr). J. Eur. Ceram. Soc. **2000**, 20 (14–15), 2619–2625.

(49) Jeitschko, W.; Nowotny, H.; Benesovsky, F. Carbides of Formula T_2MC. J. Less-Common Met. **1963**, 7, 133–138.

(50) Cabioch, T.; Eklund, P.; Mauchamp, V.; Jaouen, M.; Barsoum, M. W. Tailoring of the Thermal Expansion of $Cr_2(Al_x,Ge_{1-x})C$ Phases. **2013**, 2 (33), 897–904.

Supporting information

Table S1. Experimental a, c and z_M data for $(Zr_{1-x},Ti_x)_2(Al_{0.5}Sn_{0.5})C$ MAX phases

Method	**Ti (x)**	***a* (Å)**	***c* (Å)**	**z_M (Å)**
RHP6/30	0.00	3.344	14.568	0.088
	0.30	3.284	14.350	0.085
	0.50	3.234	14.184	0.085
	0.70	3.190	14.014	0.083
	1.00	3.115	13.714	0.082
RHP30	0.00	3.350	14.581	0.086
	0.30	3.278	14.347	0.089
	0.50	3.228	14.153	0.085
	0.70	3.187	14.007	0.083
	1.00	3.114	13.715	0.083
RHP0	0.00	3.345	14.563	0.086
	0.10	3.326	14.503	0.086
	0.30	3.279	14.343	0.087
	0.50	3.232	14.174	0.085
	0.70	3.188	13.996	0.084
	0.90	3.139	13.806	0.083
	1.00	3.115	13.707	0.082

CIP/RHP/0	0.00	3.350	14.573	0.088
	0.10	3.330	14.504	0.085
	0.30	3.283	14.341	0.090
	0.50	3.242	14.175	0.084
	0.70	3.194	13.998	0.085
	0.90	3.141	13.806	0.083
	1.00	3.116	13.709	0.080
CIP/Ar/0	0.00	3.347	14.555	0.091
	0.10	3.330	14.511	0.090
	0.30	3.299	14.360	0.085
	0.50	3.258	14.165	0.086
	0.70	3.203	14.010	0.083
	0.90	3.144	13.808	0.083
	1.00	3.108	13.713	0.081

Table S2. Tabulated CTE data of $(Zr,Ti)_2(Al,Sn)C$ measured between RT and 1500°C.

MAX Phase	Linear Fit (Å)	R^2	α ($\times 10^{-6}$ K^{-1})	α_{av} ($\times 10^{-6}$ K^{-1})	α_c/α_a	Method
$Zr_2(Al_{0.5},Sn_{0.5})C$	$a = 2.38861 \times 10^{-5} \times T(K) + 3.31194$	0.98061	*7.19(1)*	7.33	1.06	XRD
	$\mathbf{c = 1.1008 \times 10^{-4} \times T(K) + 14.42827}$	0.99337	**7.61(1)**			
$(Zr_{0.7},Ti_{0.3})_2(Al_{0.5},Sn_{0.5})C$	$a = 2.15898 \times 10^{-5} \times T(K) + 3.25486$	0.99427	*6.62(1)*	6.91	1.13	XRD
	$\mathbf{c = 1.06602 \times 10^{-4} \times T(K) + 14.23171}$	0.99849	**7.48(1)**			
$(Zr_{0.3},Ti_{0.7})_2(Al_{0.5},Sn_{0.5})C$	$a = 2.20922 \times 10^{-5} \times T(K) + 3.17773$	0.99427	*6.94(1)*	7.15	1.09	XRD
	$\mathbf{c = 1.05682 \times 10^{-4} \times T(K) + 13.91558}$	0.99502	**7.58(1)**			
$Ti_2(Al_{0.5},Sn_{0.5})C$	$a = 2.55248 \times 10^{-5} \times T(K) + 3.09115$	0.99142	*8.23(1)*	8.36	1.05	XRD
	$\mathbf{c = 1.17615 \times 10^{-4} \times T(K) + 13.60349}$	0.99805	**8.62(1)**			

Ti_2AlC			*7.1(3)*	8.07	1.41	XRD [28]
			10.0(5)			
			8.2(2)			Dilatometer[28]
Ti_2AlC			*9.0(1)*	9.2	1.07	Neutron Diffraction[29]
			9.6(1)			
			8.7			Dilatometer[30]
Ti_2SnC			10.0(2)			Dilatometer[48]
Zr_2SnC			8.3(2)			Dilatometer[48]
Ti_2SnC	$a = 2.62 \times 10^{-5} \times T(K) + 3.1591$	0.9983	*8.27(1)*	8.24	0.99	XRD
	$\mathbf{c = 1.12 \times 10^{-4} \times T(K) + 13.665}$	0.9956	**8.19(1)**			XRD

α_a in *italic*, α_c in **bold**. The number in parenthesis indicates the uncertainty on the last digit.

The O_d and P_d values for the $(Zr_{1-x},Ti_x)_2(Al_{0.5},Sn_{0.5})C$ phases calculated in this work using equations (1) and (2), along with the available literature data indicating the measurement method [22,38,40–43] are summarised in **Figure S1a and b**. A colour code was used to indicate maximum distortions (>>1) in red and minimum distortion values (≈ 1) in green. O_d/P_d ratios are tabulated in **Figure S1c** with deviations in any direction from $O_d/P_d=1$ are coloured towards red, and $O_d/P_d \approx 1$ are coloured green. The Ti_2SnC distortion values found in literature were not experimentally determined but calculated [38,40,42] and were added to **Figure S1** along with the experimentally determined values in this work. Measurement method when available was also indicated either as X-Ray Diffraction (XRD), Neutron Powder Diffraction (NPD) or Extended X-Ray Absorption Fine Structure (EXAFS). '*' indicates near phase pure ($\geq$ 95wt %) MAX phases synthesised in this work or reported in literature. The corners of the figures are occupied by the ternary carbides (end members) relevant to this study, such as Zr_2AlC, Ti_2AlC, Zr_2SnC and Ti_2SnC. In between each corner ternary MAX phase, the relevant solid solution MAX phases can be found with a composition change in Ti/Zr content in the horizontal direction, whereas the Sn/Al content changes in vertical direction.

O_d

a)

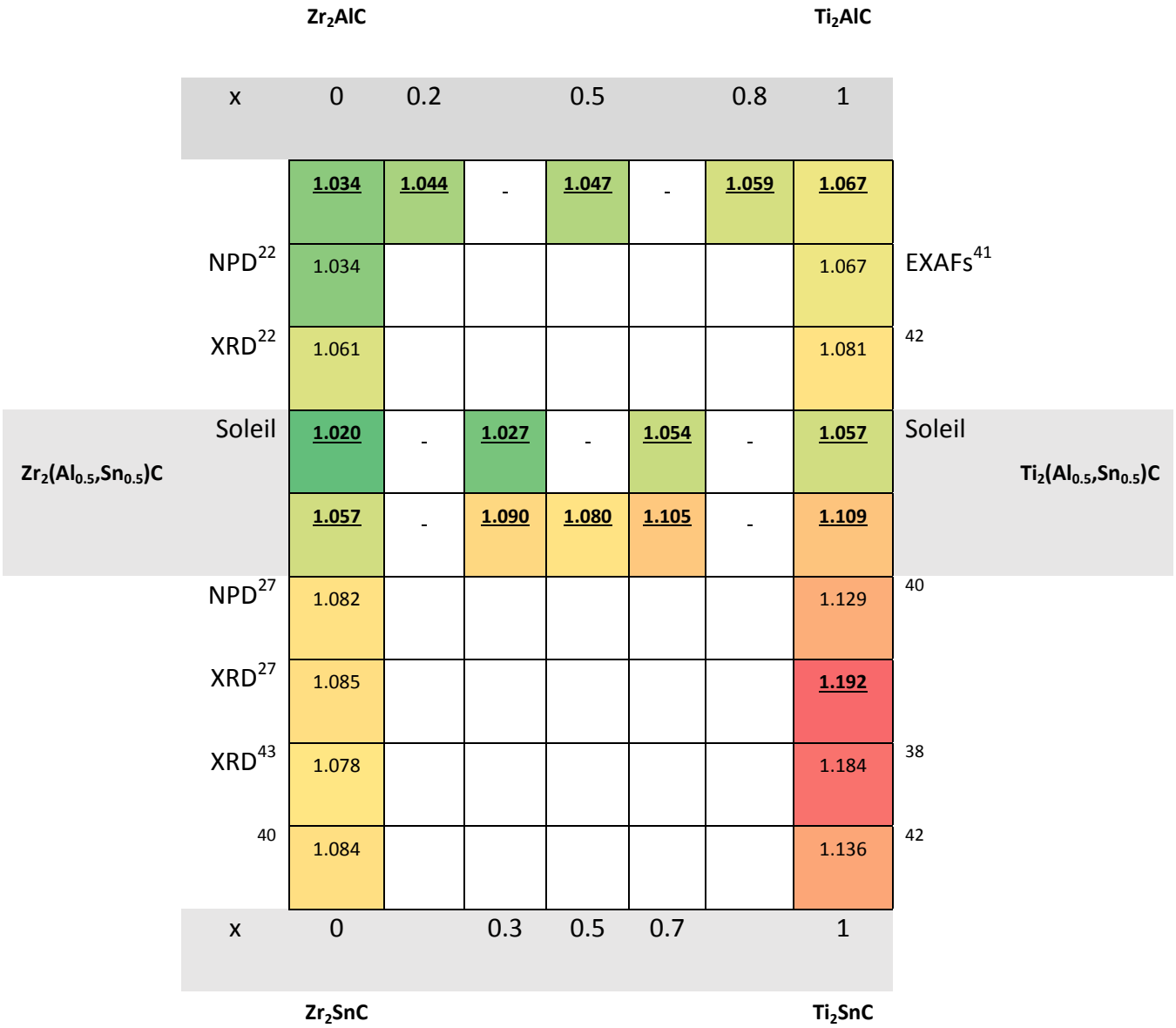
Zr2AlC
Ti2AlC
x 0 0.2 0.5 0.8 1
1.034 1.044 - 1.047 - 1.059 1.067
NPD22 1.034 1.067 EXAFs41
XRD22 1.061 1.081 42
Soleil 1.020 - 1.027 - 1.054 - 1.057 Soleil
Zr2(Al0.5,Sn0.5)C
1.057 - 1.090 1.080 1.105 - 1.109 Ti2(Al0.5,Sn0.5)C
NPD27 1.082 1.129 40
XRD27 1.085 1.192
XRD43 1.078 1.184 38
40 1.084 1.136 42
x 0 0.3 0.5 0.7 1
Zr2SnC
Ti2SnC

b)

P_d

		Zr_2AlC					Ti_2AlC	
	x	0	0.2		0.5	0.8	1	
		1.101	**1.092**	-	**1.088**	- **1.081**	**1.072**	
	NPD[22]	1.101					1.072	EXAFS[41]
	XRD[22]	1.089					1.059	42
$Zr_2(Al_{0.5},Sn_{0.5})C$	Soleil	**1.096**	-	**1.090**	-	**1.078** -	**1.073**	Soleil $Ti_2(Al_{0.5},Sn_{0.5})C$
		1.097	-	**1.081**	**1.081**	**1.071** -	**1.067**	
	NPD[27]	1.092					1.073	40
	XRD[27]	1.090					**1.058**	
	XRD[43]	1.088					1.071	38
	40	1.081					1.066	42
	x	0		0.3	0.5	0.7	1	
		Zr_2SnC					Ti_2SnC	

c) **O_d/P_d**

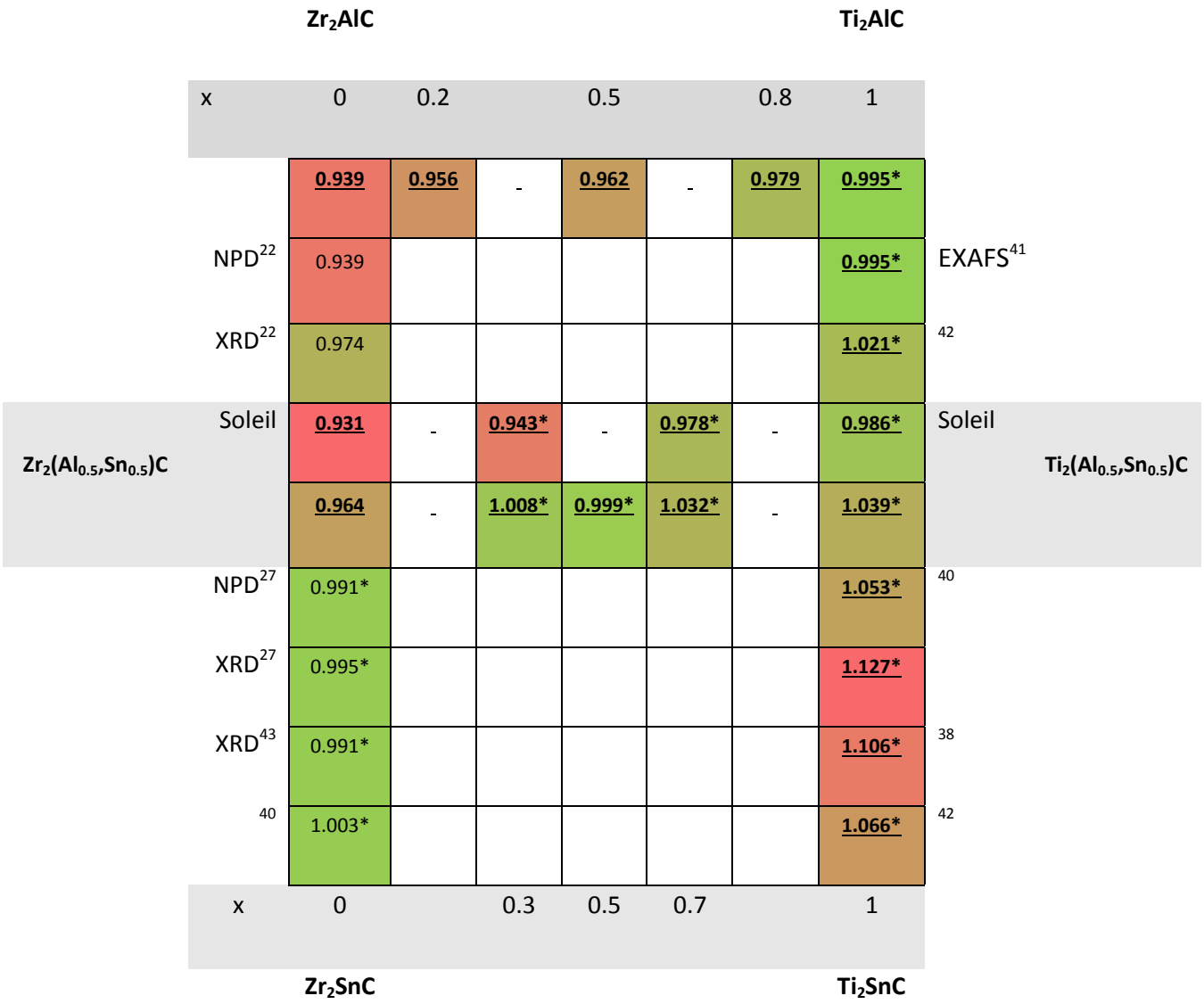

Figure S1. O_d (a), P_d (b) and O_d/P_d values for the $(Zr_{1-x},Ti_x)_2(Al_{0.5},Sn_{0.5})C$ phases synthesized with RHP6/30 calculated in this work, along with the available literature data and measurement methods. '*****' indicates the ceramics that can be produced with ≥ 95wt % phase purity. Horizontal axis is Ti content, x. The colour scale for (a) and (b) reflects the values as "high" (in red) and "low" (in green). For (c), O_d/P_d values closer to 1 is indicated as green while any deviation coloured towards red.